Rapidly Reconfigurable Optical Phase Encoder–Decoders Based on Fiber Bragg Gratings

Zhaowei Zhang, Chun Tian, Mohd R. Mokhtar, Periklis Petropoulos, David J. Richardson, and Morten Ibsen

***Abstract*—We demonstrate the capacity for fast dynamic reconfiguration of optical code-division multiple access (OCDMA) phase en/decoders based on fiber Bragg gratings and a thermal phase-tuning technique. The tuning time between two different phase codes is measured to be less than 2 s. An OCDMA system using tunable-phase decoders is compared with a system using fixed-phase decoders and, although the system using fixed-phase decoders exhibits a shorter output autocorrelation pulsewidth and lower sidelobes, the system using tunable-phase decoders has advantages of flexibility and a more relaxed requirement on the input pulsewidth.**

***Index Terms*—Code-division multiplexing, fiber-optics communication, gratings, optical fiber devices.**

I. Introduction

FIBER optical code-division multiple access (OCDMA), which combines the advantages of optical communication and access networks, has the unique features of broadband, high functionality, and security [1]. One of the key technological challenges involving OCDMA systems is how to reliably achieve code generation (encoding) and recognition (decoding). The superstructure fiber Bragg grating (SSFBG) has been shown to be an efficient all-fiber en/decoder for direct-sequence OCDMA systems [2]. It can be easily designed to encompass optical phase encoding, which provides far better performance than, for example, amplitude-only encoding [2].

To improve the functionality and flexibility of OCDMA-based optical networks, it is desirable to have en/decoders with a capacity of dynamic reconfiguration. Recently, we proposed such a tunable OCDMA phase en/decoder based on a uniform fiber Bragg grating (FBG) [3]. However, in that work, the reconfiguration function and speed was not demonstrated. Furthermore, in this work we analyze the effects of thermally induced phase shifts, which in these tunable devices are inherently distributed, on the choice of chip duration and overall system performances. The effects of this distribution have not been previously addressed.

In this letter, we experimentally demonstrate the fast (<2 s) reconfiguration capacity of an improved tunable phase encoder.

Manuscript received February 2, 2006; revised March 14, 2006.

Z. Zhang, C. Tian, P. Petropoulos, D. J. Richardson, and M. Ibsen are with the Optoelectronics Research Centre, University of Southampton, Southampton SO17 1BJ, U.K. (e-mail: zhz@orc.soton.ac.uk).

M. R. Mokhtar was with the Optoelectronics Research Centre, University of Southampton SO17 1BJ, U.K., and is now with Multimedia University, 63100 Cyberjaya, Selangor, Malaysia.

Digital Object Identifier 10.1109/LPT.2006.875062

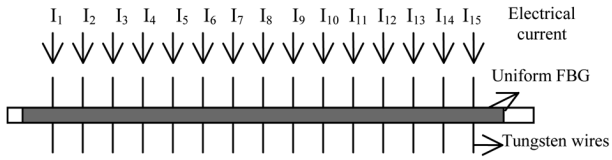

Fig. 1. Device layout of a 15-chip reconfigurable en/decoder.

Moreover, based on characterization of the phase-shift distribution of tunable en/decoders, we analyze the effects of this phase-shift distribution on system performances. The performances of a system with a reconfigurable-phase-code are experimentally compared with a system employing en/decoders with fixed-phase-codes offering discrete phase transitions.

II. Device Description and Characterization

The phase shifts in "traditional" SSFBG en/decoders are induced by a spatial gap between the uniform grating sections forming the individual chips. These phase shifts are typically discrete (shorter than the grating pitch) and cannot be tuned [2]. By applying a variation of the effective refractive index along the FBG through temperature, a phase shift on the grating can be introduced. A temperature variation of $\Delta T(x)$ applied on the fiber core of FBGs will induce a variation of $\Delta n_{\text{eff}}(x) \cong \alpha \Delta T(x)$ on its effective mode index n_{eff}, and result in a phase shift of $\phi = (4\pi/\lambda_B)\int \Delta n_{\text{eff}}(x)\,dx$, where α is the thermooptic coefficient. In this analysis, we neglect the thermal expansion effect because its contribution is only $\sim$10% of the thermooptic effect [4]. This thermal-induced phase shift is distributed because it typically covers several millimeters. The advantage is that it can easily be tuned with modest temperature changes through varying the thermal distribution.

Based on this principle, a tunable phase en/decoder with multiple equidistant phase-shifts is formed from a single uniform FBG. Tungsten wires with a diameter of 18μm, are positioned underneath the FBG, and electrical currents are controlled to pass through the individual wires. A 15-chip phase en/decoder with a chip length of 2.5 mm (corresponding to a chip duration of $\sim$25 ps) is thus constructed by positioning 15 parallel wires 2.5 mm apart along the FBG, with the first wire being placed 2.5 mm into the grating, as shown in Fig. 1. The uniform FBG is 40 mm long and is written in a standard telecom compatible fiber. As mentioned above, the phase shifts are introduced by the localized heat from tungsten wires and can be controlled by varying the electrical currents passing through the wires. This causes the temperature variation of the fiber at this point and, consequently, results in a tunable phase en/decoder.

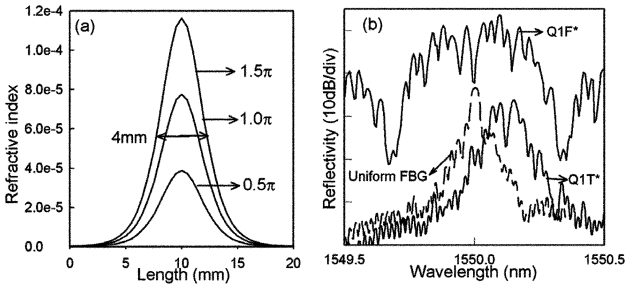

Fig. 2. (a) Distribution of a single phase shift. (b) Reflection spectra of $Q1T*$, $Q1F*$ (solid lines) and the uniform grating (dashed line).

For this particular device, to produce a phase shift of 0.5π, π, and 1.5π, the electrical currents are, respectively, 52, 70, and 84 mA [5]. Note that these current values are dependent on the wire thickness used. The distribution of effective index variation under these electrical currents was measured, and it was found that they could be approximated by a hyperbolic secant square function [5], as shown in Fig. 2(a). Its distribution length, denoted by the full-width at half-maximum, is ∼4 mm. The chip length of the tunable phase encoder is 2.5 mm, which implies that the phase shifts are not discrete and localized, and hence that the chips are coupled.

Shown in solid lines of Fig. 2(b) are measured reflection spectra of the 15-chip tunable phase decoder $Q1T*$ and the fixed phase decoder $Q1F*$, with the same phase code sequence. Their spectral inequality occurs because the phase shifts are distributed for the tunable device, while they are discrete for the fixed one. Also, shown by the dashed line, is the reflection spectrum of the uniform FBG for the tunable decoder without electrical currents.

III. Effects of Distributed Phase Shifts

Two 15-bit quaternary codes, $Q1 = [1.5\pi\ 0.0\pi\ 0.0\pi\ 0.5\pi\ 1.0\pi\ 0.0\pi\ 0.0\pi\ 1.5\pi\ 0.5\pi\ 1.5\pi\ 0.5\pi\ 0.0\pi\ 0.5\pi\ 1.0\pi\ 1.5\pi]$, and $Q2 = [1.5\pi\ 0.5\pi\ 1.0\pi\ 1.5\pi\ 0.0\pi\ 0.5\pi\ 1.5\pi\ 1.0\pi\ 0.0\pi\ 1.5\pi\ 0.0\pi\ 0.0\pi\ 0.0\pi\ 0.5\pi\ 0.5\pi]$, are chosen from the family A sequences [6]. In the first case, both the encoders $Q1F$, $Q2F$, and corresponding decoders $Q1F*$, $Q2F*$ have fixed and discrete phase shifts. In the second case, the encoders, $Q1F$ and $Q2F$, have discrete phase shifts while the decoders, $Q1T*$ and $Q2T*$, have distributed phase shifts. The Bragg wavelength, index modulation, chip length, and total length of all the gratings are, respectively, 1550 nm, 1.0×10^{-5}, 2.5 mm, and 40 mm.

The spatial phases of $Q1T$ and $Q1F$ are shown in Fig. 3(a) and (b). The phase distribution of $Q1T$ is based on the single-phase distribution shown in Fig. 2(a). Note that the distributed phase is a good approximation of the discrete one. The simulated pulse responses (when the input pulsewidth is 2 ps) of distributed-phase grating $Q1T$ and discrete-phase grating $Q1F$ are shown in Fig. 3(c) and (d). The response of $Q1T$ is a pulse with distinct edges and a smooth top-section, while that of $Q1F$ is composed of a series of short pulses divided by dips at each phase transition. The temporal phases strictly follow the spatial phases of corresponding gratings.

Shown in Fig. 3(e) is simulated autocorrelation pulse between encoder $Q1F$, and decoder $Q1T*$, while in Fig. 3(f) the decoder is $Q1F*$. There are two differences between

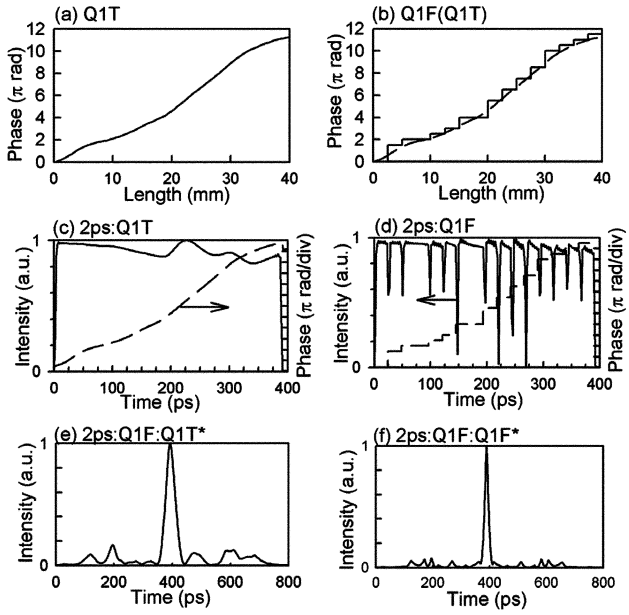

Fig. 3. Spatial phases of (a) the tunable FBG $Q1T$, and (b) SSFBG $Q1F$ (solid line) and $Q1T$ (dashed line). Intensity (solid line) and phase (dashed line) of pulse responses of (c) $Q1T$ and (d) $Q1F$. Autocorrelation pulses of (e) $Q1F$: $Q1T*$, and (f) $Q1F$: $Q1F*$.

the autocorrelation $Q1F$: $Q1T*$ and $Q1F$: $Q1F*$. First, the pulsewidth of $Q1F$: $Q1T*$ is broader than that of $Q1F$: $Q1F*$. Second, the sidelobes of $Q1F$: $Q1T*$ are higher than that of $Q1F$: $Q1F*$. Both of these differences are due to the fact that phases of encoder $Q1F$ and decoder $Q1F*$ are completely conjugate, while phases of encoder $Q1F$ and decoder $Q1T*$ are only approximately conjugate. Therefore, the decoding performance is largely dependent on specific distribution length of the distributed phases. It is obvious that the more confined the distributed phase shifts are, the better they will match the discrete phase shifts. Nevertheless, as shown in Fig. 3(e), even when the lengths of the distributed phase shifts are longer than the chip length, the autocorrelation pulse, and hence recognition signature, is still clear.

IV. Experimental Results and Discussion

The experimental setup is similar to that in [3]. A tunable laser, operated at 1550 nm, is carved through an electroabsorption modulator (driven by a 10-GHz sinusoidal signal), to produce ∼20-ps pulses, which are then gated down to 311 MHz using a $LiNbO_3$ electrooptic intensity modulator. Then this pulse train is split by a 3-dB coupler into two parts, each reflected from the fixed-phase encoders $Q1F$ and $Q2F$, respectively, and then combined by another 3-dB coupler. A fiber time delay line is utilized to divide the signals from the two encoding gratings in the time domain. Then the combined signal is reflected from the tunable decoding grating. The encoding and decoding gratings used in the experiments have the same designations and parameters as the simulation in Section III, except that the index modulation is 2.2×10^{-5}.

First, the tuning speed of the reconfigurable decoder is measured by feeding the decoded pulses into an oscilloscope having an effective detection bandwidth of 100 MHz. The reconfigurable decoder is switched from ON to OFF by controlling wire

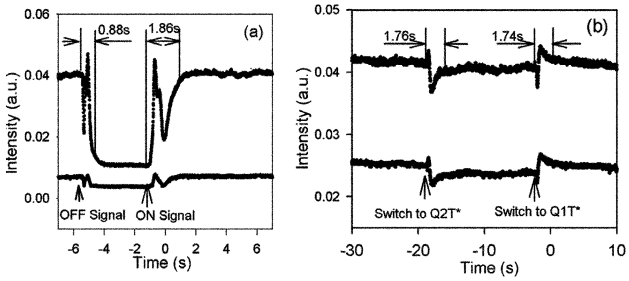

Fig. 4. Power of decoded pulses (a) when the reconfigurable decoder is switched ON–OFF–ON, (b) when the phase code sequence is switched from $Q1T*$ to $Q2T*$, and then back to $Q1T*$.

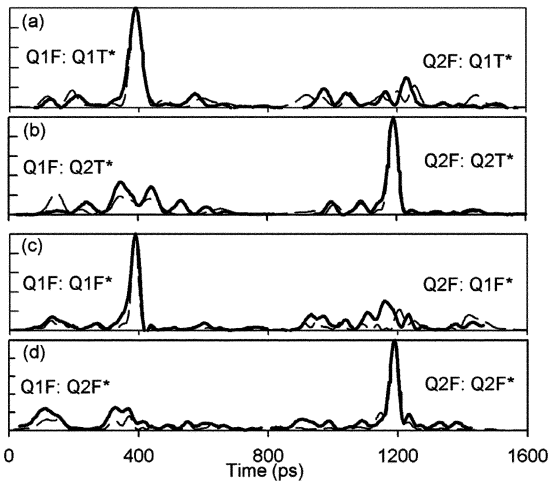

Fig. 5. Measured (solid lines) and calculated (dashed lines) decoded pulses for decoder (a) $Q1T*$, (b) $Q2T*$, (c) $Q1F*$, and (d) $Q2F*$.

currents, and then back to ON, i.e., from code to no code (uniform grating) and back to code. The power of the reflected signal (in the ON state, it is the peak of autocorrelation pulse; in the OFF state, it is measured at the background noise level) from the reconfigurable decoder is shown in Fig. 4(a). Furthermore, the phase code sequence is switched from $Q1T*$ to $Q2T*$, and then back to $Q1T*$. The power of reflected signal (including autocorrelation and crosscorrelation pulses) from the reconfigurable decoder is shown in Fig. 4(b). The response time of all the switching process is observed to be less than 2 s. This is due to the fact that the tungsten wire has a fast heat response to electrical currents, and the silica fiber used as the host for the gratings has a fast thermooptic response.

Second, the decoded pulses are detected with a 20-GHz photodiode and fed into a fast sampling oscilloscope. The measured and calculated autocorrelation and cross-correlation pulses, when the reconfigurable FBGs ($Q1T*$ and $Q2T*$) are used for decoding, are shown in Fig. 5(a) and (b). For comparison, the results obtained when the decoders are fixed-code FBGs ($Q1F*$ and $Q2F*$), are shown in Fig. 5(c) and (d). The measured ratios between the peak of cross correlation and autocorrelation are, respectively, $\sim$34% and 30% with the reconfigurable and fixed-code decoders. Then autocorrelation pulsewidths are measured by an autocorrelator, which is based on second-harmonic-generation techniques. When the decoder is a tunable FBG, the output pulsewidth is $\sim$39 ps, while when the decoder is a fixed-code FBG, it is $\sim$23 ps. Note that the input pulsewidth is $\sim$20 ps, while the chip duration is $\sim$25 ps.

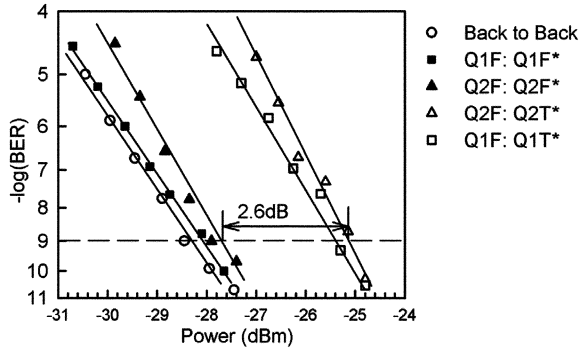

Fig. 6. BER test results for the systems which use both fixed and tunable decoders when the data bit rate is 1.25 Gb/s.

As shown in the simulation of Fig. 3, using a shorter input pulse can improve the performance of the fixed-code system, while it has no obvious effect on the tunable-code system. This we believe can be explained from Fig. 2(b), which shows that the reflection spectrum of a tunable device is narrower than that of a fixed-code device, therefore implying that the tunable device is more tolerable to a longer input pulsewidth.

Then, the bit-error rate (BER) is measured when the data bit rate is 1.25 Gb/s. These results are summarized in Fig. 6. Compared with the back-to-back case, the power penalty is $\sim$0.6 dB when the decoder is a fixed-code FBG. An additional $\sim$2.6-dB penalty is measured when the decoder is a reconfigurable FBG. This additional penalty is found mainly to be due to the increased power that exists in the shoulders of autocorrelation pulses when a distributed-phase grating is used.

V. Conclusion

We have, for the first time, demonstrated <2-s reconfiguration time of a tunable OCDMA phase en/decoder based on FBGs. The performance of a system using tunable-phase decoders is also compared with that using fixed-phase-code decoders. The system using tunable-phase decoders has a longer output autocorrelation pulsewidth and a relatively higher cross-correlation pulse. Its advantages include that it is more tolerable to longer input pulses, and has the capacity for fast dynamic reconfiguration, which is essential to improve the functionality and flexibility of future OCDMA and all-optical packet-switching networks.

References

[1] M. E. Marhic, "Coherent optical CDMA networks," *J. Lightw. Technol.*, vol. 11, no. 5, pp. 854–864, May/Jun. 1993.

[2] P. C. Teh, P. Petropoulos, M. Ibsen, and D. J. Richardson, "A comparative study of the performance of seven-and 63-chip optical code-division multiple-access encoders and decoders based on superstructured fiber Bragg gratings," *J. Lightw. Technol.*, vol. 19, no. 9, pp. 1352–1365, Sep. 2001.

[3] M. R. Mokhtar, M. Ibsen, P. C. Teh, and D. J. Richardson, "Reconfigurable multilevel phase-shift keying encoder-decoder for all-optical networks," *IEEE Photon. Technol. Lett.*, vol. 15, no. 3, pp. 431–433, Mar. 2003.

[4] R. Kashyap, *Fiber Bragg Gratings*. San Diego, CA: Academic, 1999.

[5] Z. Zhang, C. Tian, M. A. F. Roelens, M. R. Mokhtar, P. Petropoulos, D. J. Richardson, and M. Ibsen, "Direct characterization of the spatial effective refractive index profile in Bragg gratings," *IEEE Photon. Technol. Lett.*, vol. 17, no. 12, pp. 2685–2687, Dec. 2005.

[6] S. Boztas, R. Hammons, and P. V. Kumar, "4-phase sequences with near optimum correlation properties," *IEEE Trans. Inf. Theory*, vol. 38, no. 3, pp. 1101–1113, May 1992.